

Theoretical study of ion desorption from poly-(methyl methacrylate) and poly-(isopropenyl acetate) thin films through core excitation

Osamu Takahashi^{a)} and Kiyohiko Tabayashi*Department of Chemistry, Hiroshima University, Higashi-Hiroshima 739-8526, Japan*

Shin-ichi Wada, Ryouhei Sumii, and Kenichiro Tanaka

Department of Physical Science, Hiroshima University, Higashi-Hiroshima 739-8526, Japan

Michael Odelius and Lars G. M. Pettersson

FYSIKUM, AlbaNova University Center, Stockholm University, S-106 91 Stockholm, Sweden

(Received 5 July 2005; accepted 23 January 2006; published online 22 March 2006)

Site-specific chemical reactions following core excitation of poly-(methyl methacrylate) (PMMA) and poly-(isopropenyl acetate) (PiPac) thin films were investigated. New x-ray absorption spectra of PMMA and PiPac at the C and O *K* edges and theoretical spectra within the framework of density functional theory using model molecules were reported, and some new peak assignments were proposed for these spectra. Core-hole excited state molecular dynamics simulations were performed to discuss dissociation dynamics for the target systems, and some specific reaction mechanisms were discussed and explained theoretically; for example, the amount of CH₃ ion fragments for PMMA was enhanced at the C and O *K* edges through the existence of the repulsive $\sigma^*(\text{O}-\text{CH}_3)$ excited state. © 2006 American Institute of Physics. [DOI: 10.1063/1.2176605]

I. INTRODUCTION

To control the scission of a specific chemical bond is one of the dreams of chemists. In mid-1980s, a site-specific chemical reaction induced by soft x-ray radiation was suggested by Eberhardt *et al.*¹ Following their pioneering work, many investigations have been reported about characteristic chemical reactions such as specific chemical bond scission and molecular elimination by soft x-ray radiation, which could not be observed by valence excitation.^{1–13} Several reaction mechanisms following core excitation have been proposed.^{14–18} Except for some special cases, such as the two-step bond scission mechanism deduced from angular correlations in molecular Auger decay of CO after C(1s) excitation,¹⁹ it is believed that these chemical reactions proceed successively under three processes:^{20–22} (1) photoabsorption, (2) energy relaxation, among which the Auger decay process is dominant for lighter elements,²³ and (3) bond dissociation (chemical reaction). By tuning the excitation energy in the photoabsorption, the initial states of the reaction can be selected. The core electrons are localized on an atom, and the core-excitation energy reflects the surrounding chemical environment of the atom. The excitation energy thus depends on the position of the atom in the molecule; with high resolution spectroscopy, a specific atom can be selectively core excited. The relaxation processes after the core excitation are also expected to be site specific. Because the core hole is localized the electrons participating in the Auger decay should be located near the core hole. A specific chemical bond will then become weakened through decay of electrons from valence orbitals which contribute to that bond.^{7,24,25}

The core hole, furthermore, depending on the atomic

species, has a lifetime of a few femtoseconds. Since the effect of the core hole on the valence electrons can be described through the equivalent core or *Z*+1 approximation where the reduced screening is modeled by increasing the nuclear charge by one unit, we can expect that core ionization and excitation will lead to a change in geometry. If the induced gradient is sufficiently strong we can expect that the Auger final state configurations will be different from the initial ground state and thus not representative of configurations probed by photoexcitation in the valence region.^{26,27} Although we cannot control such a decay process, the core-excited state, which induces the specific Auger decay, weakening one or some specific chemical bonds, can be selected by tuning the photon energy. Thus it is important to examine the character of the excited state and the decay process as basis for a discussion of state specificity and site selectivity in the chemical reaction following the core excitation. In order to explore the reaction mechanisms experimentally, various multicoincidence techniques, such as photoelectron-photoion coincidence³ (PEPICO) and Auger electron-photoion coincidence (AEPICO) techniques,¹⁰ have been developed both for surface adsorbed and gas phase systems.

In several studies of chemical reaction following core excitation stimulated by the initial papers the poly-(methylmethacrylate) (PMMA) thin film has provided a typical example for which significant core-excitation-induced site-specific chemical reactions have been observed. Tinone *et al.*¹³ and Tanaka *et al.*²⁰ showed that the amount of dissociated fragments could be varied by tuning the photon energy at the C and O *K* edges. For instance, at the O *K* edge, enhancement of CH₃⁺ ion desorption was detected when the excitation photon energy was around 532 eV, while enhancement of OCH⁺ ion desorption as decomposition product of the parent ion OCH₃⁺ was detected around 540 eV. In subse-

^{a)}Electronic mail: shu@hiroshima-u.ac.jp

quent studies by the same group, site-specific bond scission to yield CH_3^+ ions was also reported using the AEPICO technique.^{6,8}

In those papers, the importance of the repulsive character of the core-excited state and of the repulsive two-hole/one-electron Auger final state was emphasized while determining the scission of specific chemical bonds. However, the peaks in the PMMA x-ray absorption (XA) spectrum have not been unambiguously assigned. As another motivation for the present study, site-specific chemical reactions around the ether O atom have also been observed for poly-(isopropenylacetate) (PiPac) thin films at the O K edge, which is a structural isomer of PMMA.²⁸ Contrary to PMMA, the COCH_3^+ ion yield was increased, while that of OCOCH_3^+ ion was unaffected by variations in the excitation energy. These differences in the reactivity between PMMA and PiPac are still not understood. One of our objectives is thus to analyze the reaction mechanism for these kinds of polymers from a theoretical viewpoint. Furthermore, the XA spectrum of PiPac at the C K edge has not been reported previously. In order to understand in a systematic way the reactivity of PMMA and PiPac after core excitation, it is important to specify the peak positions and assign the XA spectra. The second objective is to compute the XA spectra of PMMA and PiPac at the C and O K edges to compare the theoretical spectra using model molecules with the new experimental data.

Previously, we have reported theoretical investigations of the reaction mechanism for site-specific chemical reactions following core excitation for a series of methylcyano esters and ketones using *ab initio* molecular orbital (MO) and density functional theory (DFT) calculations.^{24,25,29} In those papers, the molecular size dependence of chemical reaction following core excitation could be explained theoretically for methylcyano esters and ketones, i.e., the ion yield depends on the distance from the excited atom. Sako *et al.* have previously discussed the reaction mechanisms for PMMA thin films after Auger decay using a model monomer,⁷ and suggested the importance of Auger final states which have holes in the bonding orbitals of the chemical bond which undergoes scission. In the present paper, we concentrate the discussion on the assignment of XA spectra and the influence of the dynamics on the reaction mechanism in the core-hole state.

Recent development of theoretical approaches in the field of inner-shell excitations is remarkable. Typical molecules that are of experimental interests for site-specific chemical reactions following core excitation are too large for calculations of the excited states using molecular *ab initio* calculations based on the configuration interaction (CI) or the symmetry adapted cluster-configuration interaction (SAC-CI) methods.³⁰ In this case the transition potential (TP) DFT-based³¹ method offers a good alternative technique to compute core-excited photoabsorption spectra. This procedure has been widely applied to systems ranging from relatively small molecules in the gas phase^{31–33} to large systems such as surface adsorbed molecules using cluster models³⁴ and to models of liquid water and ice.^{35,36}

In the present study, theoretical calculations of XA spectra using the DFT-TP methodology were performed in order

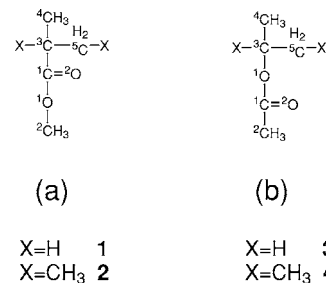


FIG. 1. Model molecules of poly-(methyl methacrylate) (PMMA) (left) and poly-(isopropenyl acetate) (PiPac) (right). **1** and **3** correspond to $X=\text{H}$ and **2** and **4** correspond to $X=\text{CH}_3$.

to examine the character of the excited states and to discuss the reactivity of PMMA and PiPac at the core-excited level. We focus especially on bond scission in the core-hole state although most of the dissociation processes after core excitation depend on the dynamics on the potential energy surface of the Auger final states. However, it is important to trace the successive processes step by step and the initial dynamics in the core-hole state preceding the Auger decay leading to the final valence ionized and excited state provides an essential difference compared to an excitation to the same electronic configuration by direct photoionization.

II. COMPUTATIONAL PROCEDURE

Two kinds of molecular models were used to represent the PMMA and PiPac polymers. The main chain of model molecules **1** and **3** was terminated by two hydrogen atoms, and that of model molecules **2** and **4** was terminated by two methyl groups. Geometry optimization for these model molecules (see Fig. 1) were performed using GAUSSIAN 98 (Ref. 37) at the MP2/cc-pVDZ level of approximation. The XA spectra depend on the chemical environment around an excited atom.³⁸ In the present study, model molecules **2** and **4** were used to produce XA spectra theoretically and **1** and **3** were used to investigate the reaction mechanism of ion desorption.

The detailed computational procedure has already been described elsewhere.^{31,32,39} In short, the theoretical XA spectra were generated by the TP method^{40,41} in combination with a double basis set technique.⁴² The orbitals for the molecule were determined using a good quality molecular basis set with a half-occupied core orbital at the ionization site. The orbitals for the excited electron were then obtained by diagonalizing the Kohn-Sham matrix built from the former density in a basis set extended by a large set of diffuse basis functions (150–400 functions) centered on the excited atom. The obtained orbital energies and computed transition moments provide a representation of the excitation energies and associated intensities in the theoretical spectrum.

The TP calculation gives most of the relaxation effect upon core ionization and provides a single set of orthogonal orbitals for the spectrum calculation. The DFT-TP calculation of the spectrum corresponds to the static exchange (STEX) approach^{43,44} and thus neglects the relaxation effects on the molecular ion core on adding the excited electron. This effect is largest for the valencelike π^* excitations and,

therefore, these states are computed with fully relaxed Δ Kohn-Sham (Δ KS) calculations. In order to determine the absolute energy position of the excited states, Δ KS calculations, i.e., allowing full relaxation of the fully ionized core-hole state, were performed to compute the relaxed ionization potential (IP) energy. The core-excited states were variationally determined with maintained orthogonality between the excited states through the following procedure. The first excited state was obtained by fixing the occupation of the core spin-orbital to zero and placing the excited electron in the first unoccupied orbital. A full relaxation with this constraint leads to a state that is near orthogonal to the ground state due to the $1s^{-1}$ configuration. The next state was then obtained by removing the variationally determined excited orbital from the variational space and occupying the next level. This procedure gives a variational lower bound to the energy and guarantees orthogonality between the excited states since all the remaining orbitals now have to be orthogonal to the successively defined and eliminated levels.³² The corresponding peaks in the energy-shifted TP spectrum have been shifted to include the additional relaxation effects obtained from these specific Δ KS excited state calculations. Relativistic effects on the IP of 0.08 eV for the C K edge and 0.33 eV for the O K edge³³ were added to produce the overall shift of the spectrum. In the Δ KS and TP calculations the noncore-excited C or O atoms were described by effective core potentials (ECPs).⁴⁵ This simplifies the definition of the core-hole state, since the use of an ECP description eliminates the $1s$ level of the atom to which it is applied. This is very helpful in core-hole calculations for an atom, which is not the only one of its kind in the studied molecule. The ECPs introduce insignificant effects on the computed spectrum.

In order to obtain an improved representation of relaxation effects in the inner orbitals, the ionized center was described by the IGLO-III basis of Kutzelnigg *et al.*⁴⁶ In the spectrum calculations a large [$19s\ 19p\ 19d$] diffuse even-tempered augmentation basis set centered on the ionization site was added; it is employed only in the last step of the calculation when the orbitals for the excitations have to be generated. The spectrum was generated by a Gaussian convolution of the discrete spectrum with varying broadenings. For the region below the ionization threshold the broadening [full width at half maximum (FWHM)] was 0.7 eV at the C K edge and 1.0 eV at the O K edge; for the next 12 eV the FWHM was linearly increased up to 4.0 eV. The stability of the convoluted spectra with respect to the augmentation basis was investigated by extending the augmentation basis to include the excitation basis also on the nearest neighbors.

The ground state geometry does not necessarily correspond to the optimum geometry of the core-excited state and we can expect that, during the core-hole lifetime, the system will begin to move towards the excited state minimum geometry.²⁶ In order to examine this effect on the core-hole state, the DFT level molecular dynamics (MD) simulations were performed on the Born-Oppenheimer potential energy surfaces of the core-excited states of PMMA and PiPac at the C and O K edges; the forces were obtained from the STOBE molecular local basis set code.⁴⁷ The three lowest resonant excited states were examined, since the lower exci-

tation states are of importance to the bond scission of CH_3 ions from PMMA, which is the most interesting ion desorption reaction in these polymers. The MD simulations were started with the nonvibrating molecule in the ground state equilibrium geometry at 0 K. We model the excitation in the sudden approximation, i.e., the excited state dynamics is initiated at the ground state equilibrium geometry. A long time step, Δt , of 1 fs was used. Although this may seem too long as time step in the MD simulation, tests with shorter time steps indicate that the induced numerical errors were very small over the 20 fs simulated. The Verlet algorithm was used as integrator of the equations of motion. The simulations were run for 20 fs, which is sufficiently long for our objective since the short core-hole lifetime, 3–6 fs, for the second-row elements ensures that most core-excited states will have decayed within this time.

All DFT calculations were performed with the gradient-corrected Perdew and Wang exchange-correlation functional.⁴⁸ All DFT calculations for the XA spectra and dynamics were performed at the gradient-corrected DFT level using the STOBE-DEMON program.⁴⁷

III. EXPERIMENTAL METHODS

Measurements of XA spectra of PMMA and PiPac at the C and O K edges were performed on the soft x-ray beam line BL-13 at HISOR of Hiroshima University. Thin films of both samples were prepared by spin casting on Au coated Si(100) substrates. The pressure of the experimental chamber was kept at the 10^{-10} Torr range. The XA spectra were obtained by measuring a sample drain current [total electron yield (TEY)] and corrected for fluctuations in synchrotron radiation (SR) light intensity. All measurements were performed with the spectral resolving power ($E/\Delta E$) of about 1500 and 1000 at the C and O K edges, respectively. Photon energy was calibrated by the intense π^* resonance of highly oriented pyrolytic graphite⁴⁹ (HOPG) and Rydberg transitions of gaseous CO_2 ,⁵⁰ and positions of resonant states measured for PMMA and PiPac were reassigned. During the measurements, no effects of irradiation damage of the samples were observed.

IV. RESULTS AND DISCUSSION

A. XA spectra of PMMA and PiPac

We begin by discussing the computed C K edge XA spectra of PMMA shown in Fig. 2. The summed spectrum for the five distinct carbon atoms in a monomer unit (model molecule 2) and the experimental spectrum are shown, and the proposed peak assignments are listed in Table I. The correspondence between experiment and our theoretical values is rather good. We would like to describe some specific peaks of the spectra. A shoulder of the summed spectra at 287.2 eV (Fig. 2) is assigned to C^4 or $\text{C}^5 \rightarrow \sigma^*(\text{C}-\text{H})$, which is mainly related to the main chain carbons. This peak was previously assigned to a C^4 or $\text{C}^5 \rightarrow \sigma^*(\text{C}-\text{C})$ excitation, but a more recent experiment has given a modified assignment as due to a $\text{C} \rightarrow \sigma^*(\text{C}-\text{H})$ excitation.⁵¹ A sharp main peak at 287.6 eV is assigned to $\text{C}^1 \rightarrow \pi^*(\text{C}=\text{O})$. The first peak at 288.4 eV is also assigned to a $\pi^*(\text{C}=\text{O})$ excitation from C^2

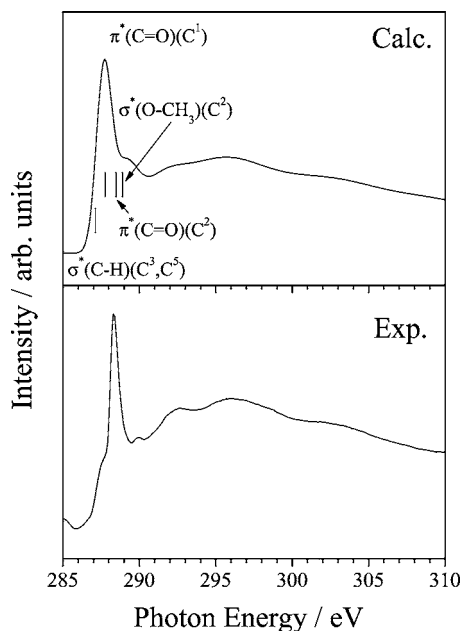


FIG. 2. Theoretical and experimental XA spectra of PMMA at the C *K* edge. The assignments of some peaks are also shown.

experimentally; however, since the intensity of this excitation is relatively smaller than that from C¹, this peak becomes a shoulder in the summed spectrum of calculation. It should be noted that the excited state assigned to C² → σ*(O-CH₃) is found at 288.9 eV, which is a slightly

higher energy than the main peak of the summed spectrum. Other broad structures are assigned as follows: a small peak at 290.0 eV is assigned to C² → σ*(C-H), a broad peak around 292 eV is assigned to C¹ → σ*(C-C), and broad structures in the continuum around 296 and 303 eV are considered as mainly arising from C¹ → σ*(C-OCH₃) and σ*(C=O), respectively. The computed ionization thresholds for each carbon are also shown in the same table.

In Fig. 3 we show the computed C *K* edge XA spectrum of PiPac obtained using model molecule **4** and the proposed peak assignments are included in Table I. PMMA and PiPac are structural isomers differing only in the position of an ether O atom and a C=O functional group. Since PiPac and PMMA contain the same functional groups we expect that the spectra should be similar as is also found by comparing the shape of the summed spectrum for PiPac with that of PMMA, but there are some differences induced by the different chemical environments. A shoulder in the main peak at 287.1 eV is assigned to C³ and C⁵ → σ*(C-H) excitations. The intensity of the main peak at 287.9 eV, assigned to a C¹ → π*(C=O) excitation, becomes relatively smaller in PiPac. Contrary to the case of PMMA, however, no excited state of σ*(C-CH₃) character, which is expected to contribute to methyl ion desorption, could be found in the PiPac spectrum. Note that an excited state that is assigned to a C³ → σ*(C-OCOCH₃) excitation exists at 288.9 eV, suggesting that it may be possible to selectively cleave a C-O chemical bond of PiPac through inner-shell excitation. A

TABLE I. Photon energies and assignments for the peaks calculated and observed in the excitation of PMMA and PiPac thin films at the C *K* edge.

Calc.		Expt. ^a	
Energy (eV)	Assignment	Energy (eV)	Assignment
PMMA			
287.2	σ*(C-H)(C ^{4,5})	287.7	σ*(C-H)/Rydberg
287.6	π*(C=O)(C ¹)	288.4	π*(C=O)(C ¹)
288.9	σ*(O-CH ₃)(C ²)	288.8	σ*(O-CH ₃)(C ²)
290.0	σ*(C-H)(C ²)	290.0	σ*(C-H)(C ²)
290.8	IP(C ^{4,5})		
291.2	IP(C ³)		
292.4		292.5	σ*(C-C)(C ^{3,4,5})
292.7	IP(C ²)		
294.2	IP(C ¹)		
296		296.0	σ*(C-OCH ₃)(C ¹), σ*(C-C)(C ^{3,4,5})
303		303	σ*(C=O)(C ¹)
PiPac			
287.1	σ*(C-H)(C ^{3,5})	287.7	σ*(C-H)/Rydberg
287.9	π*(C=O)(C ¹)	288.6	π*(C=O)(C ¹)
288.9	σ*(C-OCOCH ₃)(C ³)	288.7	σ*(C-OCOCH ₃)(C ³)
289.2	σ*(C-H)(C ²)	289.8	σ*(C-H)(C ²)
290.8	IP(C ^{4,5})		
291.4	IP(C ³)		
292.0		293.2	σ*(C-C)(C ^{4,5})
292.4	IP(C ²)		
294.4	IP(C ¹)		
297		297.1	σ*(C-C)(C ^{4,5}), σ*(O-COCH ₃)(C ¹)
303		303.3	σ*(C=O)(C ¹)

^aThis work.

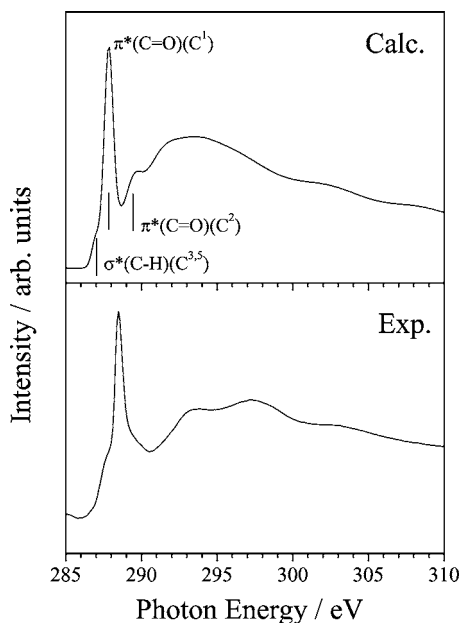


FIG. 3. Theoretical and experimental XA spectra of PiPac at the C *K* edge. The assignments of some peaks are also shown.

small shoulder at 289.2 eV is assigned to $C^2 \rightarrow \sigma^*(C-H)$ excitation. The broad structures in the continuum around 297 and 303 eV are also reproduced theoretically and are considered as mainly arising from $C^1 \rightarrow \sigma^*(O-COCH_3)$ and $\sigma^*(C=O)$, respectively. Ionization thresholds for each carbon are also shown in the table.

The computed O *K* edge XA spectra of PMMA using model molecule **2** are shown in Fig. 4. The first sharp peak at 532.1 eV is assigned to $O^2 \rightarrow \pi^*(C=O)$, in agreement with the experimental assignment. The second peak at 535.2 eV is assigned to $O^1 \rightarrow \pi^*(C=O)$. This peak has been assigned to $O^2 \rightarrow \sigma^*(C-OCH_3)$ experimentally¹³ however, from our calculations we cannot find any significant contributions from O^2 excitations to $\sigma^*(C-OCH_3)$ that could contribute to chemical bond breaking. Similar to PMMA at the C *K* edge, an excited state assigned to $O^1 \rightarrow \sigma^*(O-CH_3)$ is found at 535.8 eV. From experiment, a broad large peak at 540.3 eV was assigned to $O^1 \rightarrow \sigma^*(C-OCH_3)$. It is difficult to calcu-

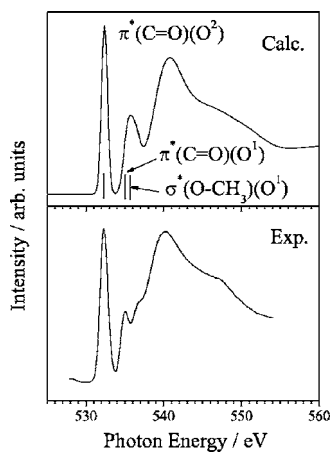


FIG. 4. Theoretical and experimental XA spectra of PMMA at the O *K* edge. The assignments of some peaks are also shown.

TABLE II. Photon energies and assignments for the peaks calculated and observed in the excitation of PMMA and PiPac thin films at the O *K* edge.

Calc.		Expt. ^a	
Energy (eV)	Assignment	Energy (eV)	Assignment
PMMA			
532.1	$\pi^*(C=O)(O^2)$	532.3	$\pi^*(C=O)(O^2)$
535.2	$\pi^*(C=O)(O^1)$	535.0	$\pi^*(C=O)(O^1)$
535.8	$\sigma^*(O-CH_3)(O^1)$	536.4	$\sigma^*(O-CH_3)(O^1)$
537.5	IP(O^2)		
538.7	IP(O^1)		
540.5		540.3	$\sigma^*(C-OCH_3)(O^1)$
546		547.6	$\sigma^*(C=O)(O^2)$
PiPac			
531.9	$\pi^*(C=O)(O^2)$	532.3	$\pi^*(C=O)(O^2)$
534.6	$\pi^*(C=O)(O^1)$	534.8	$\pi^*(C=O)(O^1)$
535.3	$\sigma^*(C-OCOCH_3)(O^1)$	536.8	$\sigma^*(C-OCOCH_3)(O^1)$
536.3	Rydberg(O^1)		
537.5	IP(O^2)		
538.7	IP(O^1)		
541		541.6	$\sigma^*(O-COCH_3)(O^1)$
548		547.6	$\sigma^*(C=O)(O^2)$

^aThis work.

late the excited state in this energy region by the Δ KS method, because the excitation energy is almost at the IP threshold and many Rydberg-type excited states exist in this region. We tried to calculate ten excited states, but no excited state assignable to $O^1 \rightarrow \sigma^*(C-OCH_3)$ was found; this state may still exist at a higher energy. Ionization thresholds for each oxygen atom are also shown in Table II.

The O *K* edge XA spectra of PiPac using model molecule **4** are shown in Fig. 5. The first sharp peak at 531.9 eV is assigned to $O^2 \rightarrow \pi^*(C=O)$, in agreement with the assignment from experiment. The next small peak at 534.6 eV is assigned to $O^1 \rightarrow \pi^*(C=O)$. Similar to the case of PMMA, we find the excited state assigned to $O^1 \rightarrow \sigma^*(C-OCOCH_3)$ at 535.3 eV, with a different character than the previous $O^2 \rightarrow \sigma^*(C-C)$ assignment.²⁸ The next small peak is due to an $O^1 \rightarrow$ Rydberg excitation, but no state assignable to $O^1 \rightarrow \sigma^*(O-COCH_3)$ is found from the calcu-

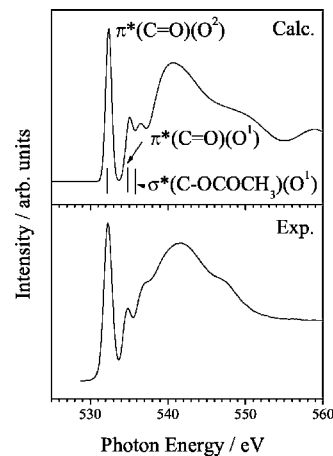


FIG. 5. Theoretical and experimental XA spectra of PiPac at the O *K* edge. The assignments of some peaks are also shown.

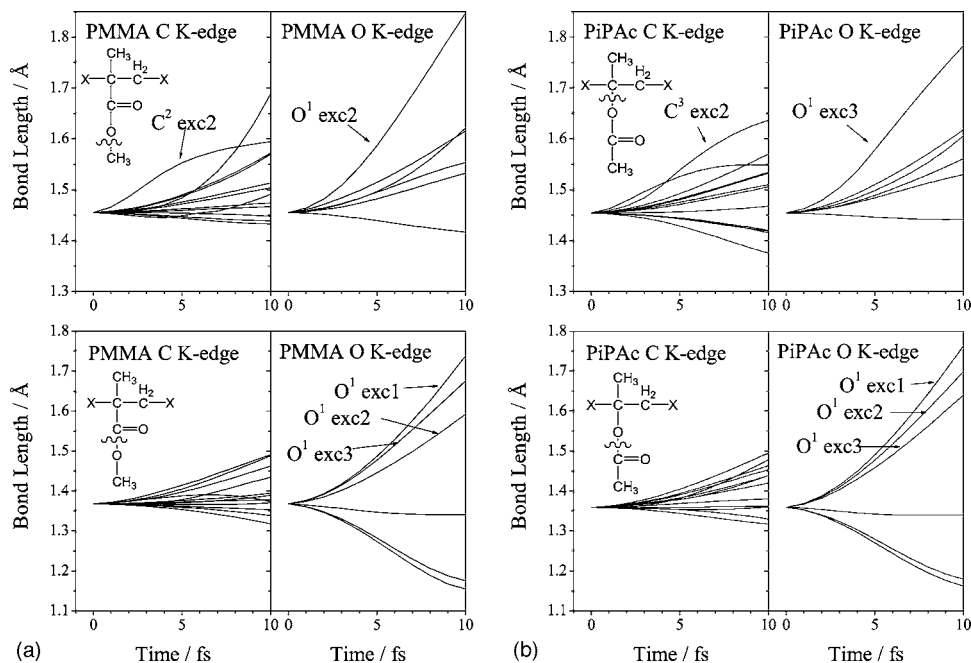


FIG. 6. C–O bond dynamics of PMMA and PiPac at the C and O K edges from CHES MD simulation. (a) PMMA by the model molecule **1**. (b) PiPac by the model molecule **3**.

lations. Ionization thresholds for each oxygen are also shown in Table II.

In summary we find that our computed XA spectra correspond quite well to experiment and propose some new peak assignments. Some hidden states assignable to the repulsive σ^* excited state were able to be found from our calculations. In the context of excitation-induced fragmentation reactions it should, in particular, be emphasized that the dissociative $\sigma^*(\text{O}-\text{CH}_3)$ excited states of PMMA are found both experimentally and theoretically.

B. Ion desorption from PMMA and PiPac

In this section, we would like to discuss the chemical reactions of PMMA and PiPac following the core excitation. In order to simulate the dynamical effect on the core-hole state, core-hole excited state (CHES) MD simulations without any constraints on the degrees of freedom were performed for the low-lying three resonant core-excited states from each core atom to examine the dynamical process. Because the low-lying resonant core-excited state still remains a valence type of character, it is expected that the site specificity will be enhanced more effectively by the core-excited electron. On the other hand, for higher resonant core-excited states, mixing with Rydberg states becomes dominant and the effects on the subsequent dynamics will be less dependent on the specific excited orbital. The hydrogen terminated model molecules **1** and **3** were used for simplicity. All MD simulations were started from the equilibrium geometry at the ground state with the nonvibrating molecule. The present discussion will be focused on bond scissions of C–O chemical bonds in PMMA and PiPac.

The C–O bond dynamics of PMMA for model molecule **1** is presented in Fig. 6(a). Owing to the character of excited states, changes of C–O bond length are different for each excited state even if the starting geometry is the same. For the O–CH₃ bond, there are two significant dissociative excited states at the second resonant state from C² excitation

(C² exc2 in the figure) and the first resonant state from O¹ excitation (O¹ exc1), where the assignments of the excited states are C² and O¹ \rightarrow $\sigma^*(\text{O}-\text{CH}_3)$. On these repulsive potential surfaces, the O–CH₃ bond is elongated about 0.1 Å at C and O K edges within the core-hole lifetime, 6.9 fs for C(1s) (Ref. 52) and 4.1 fs for O(1s).³⁰ The C–O bond elongation is accelerated at the O K edge more than at the C K edge, indicating that it is more efficient to excite a heavier atom in order to accelerate the bond elongation on the core-excited state. For the C–OCH₃ bond, bond elongations at the C K edge are less effective depending on the character of the excited states. At the O K edge, the C–O bond elongation is accelerated for three resonant excited states from the ether O¹ atom. However, significant ion desorption of OCH_n⁺ ion was not observed experimentally around the excitation energy we investigated by the core-hole excited state MD simulations. It thus seems that the CH₃ ion desorption is much faster or that neutral fragmentation of OCH_n may occur instead.

C–O chemical bond elongations of PiPac for model molecule **3** are shown in Fig. 6(b). We discuss O–COCH₃ and C–OCOCH₃ bond scissions at the O K edge. As for the case of PMMA at the O K edge, it is expected that O–COCH₃ bond scission is accelerated at the O¹ excitation due to the similar chemical environment around the C–O bond; this is consistent with the experiment by Fujii *et al.* Furthermore, according to their experiments, the yield of CH₃⁺ ion was also enhanced in the same excitation energy region, suggesting that secondary bond scission from COCH₃⁺ ion occurs and CO and CH₃⁺ ions are produced. On the other hand, a selective increase of the amount of OCOCH₃⁺ ion was not observed experimentally even if a large bond elongation for the third resonant excitation from O¹ core excitation is predicted. Detection of this ion may be achieved by high resolution experiments. We can also predict the reactivity of PiPac at the C K edge. In a similar way to PMMA, O–COCH₃ bond scission will not be accelerated at

TABLE III. Bond length elongation (in Å) of C–N bonds after 20 fs from CHES MD simulations of PMMA and PiPac. Model molecules **1** and **3** are used and the results for the three lowest core-excited states are shown.

Core hole	PMMA			PiPac		
	Energy ^a	$\Delta R(\text{O}-\text{CH}_3)$	$\Delta R(\text{C}-\text{OCH}_3)$	Energy ^a	$\Delta R(\text{O}-\text{COCH}_3)$	$\Delta R(\text{C}-\text{OCOCH}_3)$
Eq. ^b		1.455	1.368		1.359	1.454
C ¹	287.8	-0.007	0.189	287.0	0.158	0.038
C ¹	291.1	0.096	0.028	287.7	0.020	0.136
C ¹	291.6	0.385	-0.096	287.8	-0.106	0.374
C ²	288.6	1.091	-0.089	289.2	0.055	0.063
C ²	289.0	0.011	0.159	289.4	0.015	0.079
C ²	289.2	0.050	0.264	289.5	-0.019	0.136
C ³	287.8	-0.003	0.255	287.2	0.322	-0.081
C ³	288.0	0.073	0.082	287.8	0.217	0.112
C ³	288.7	0.405	-0.084	288.0	0.240	0.087
C ⁴	287.0	0.016	0.001	288.0	0.109	-0.056
C ⁴	287.6	-0.016	0.073	291.4	0.198	-0.108
C ⁴	287.7	0.011	0.026	292.0	0.148	-0.057
O ¹	535.4	0.033	1.024	535.1	1.069	0.048
O ¹	536.1	0.759	0.847	535.6	0.798	0.403
O ¹	536.3	0.275	0.811	536.2	0.698	0.531
O ²	532.5	0.0	-0.004	532.4	-0.003	0.027
O ²	536.1	0.259	-0.114	534.7	-0.131	0.351
O ²	535.5	0.353	-0.013	535.4	-0.044	0.425

^aExcitation energies (in eV) at the starting point of the core-hole excited state MD simulation.

^bBond distances at the equilibrium geometry.

the C *K* edge because the significant fast elongation of the O–COCH₃ bond cannot be observed on the core-hole excited states as far as we examined. For the C–OCOCH₃ bond scission, it may be possible to observe the site-selective bond scission in the same manner as for PMMA. Note that fast bond elongation for a C–CH₃ bond of PiPac was not obtained for any resonant excited states at the C and O *K* edges (not shown), indicating that C–C bond cleavage is not accelerated in the core-excited state.

Bond lengths of C–O bonds from the CHES MD simulations of PMMA and PiPac after 20 fs time propagation are listed in Table III. Although time propagation of 20 fs is much longer than the core-hole lifetime at the C(1s) and O(1s) excitations, it is suitable to enhance the effect of the bond elongation on the repulsive potential surface, i.e., the target chemical bond will get longer and longer on the repulsive potential. We find a strongly dissociative trajectory for the first resonant core-excited state after the C² excitation of PMMA, in agreement with the conclusion obtained through the above consideration. During the MD simulations, two potential energy surfaces intersect involving the second strongly repulsive and the first bound state, leading to a switch in the order of the potential surfaces. For the remaining carbon core-excited states, no strongly dissociative trajectories were found. These results correspond to the experimental results at the C *K* edge.

The situation for the O *K* edge of PMMA is more complicated. Dissociative trajectories leading to CH₃⁺ are found for the second and third excited states upon both O¹ and O² excitations. These results correspond to the experimental results, i.e., that the amount of methyl ion increased at about 536 eV. However, we find a dissociative trajectory leading to OCH₃ for the first excited state upon O¹ excitation. Note that

the excitation energy of this state is similar to the second and third excited states in the case of O² excitation. For the dissociation channel, CH₃ ion detection is preferred over OCH₃ ion due to the neutral fragmentation for a heavier fragment. Experimentally, at higher excitation energy (around 540 eV), the amount of OCH₃⁺ ion, which should be derived from OCH₃⁺ ion, was enhanced. We cannot perform a theoretical calculation to explain this effect explicitly because the core-excited states near the ionization thresholds cannot be obtained, but consideration of the potential energy surfaces suggests an explanation of this observation. Since all calculated potential surfaces for the C–OCH₃ bond in the O *K* edge excited states are repulsive from the preliminary calculations, while those for the O–CH₃ stretch, especially at higher excitation energy, are attractive the dissociative feature of the O–CH₃ bond will be weakened by increasing the excitation energy, while that of the C–OCH₃ bond can be expected to be enhanced.

For PiPac at the C *K* edge, ion desorption experiments have not been performed in this energy range, but based on our theoretical analysis site-specific bond scission is not expected. At the O *K* edge, specific bond scission around the ether O atom is predicted also for PiPac; however, this bond scission is not as evident as for the case of PMMA. The difference between PMMA and PiPac in postexcitation reactivity is mainly due to the chemical environment around the ether O atom or due to neutral fragmentation.

V. SUMMARY

In the present paper, site-specific chemical reactions following core excitation of PMMA and PiPac were discussed theoretically within the framework of DFT. The experimental

XA spectra of PMMA and PiPac were able to be reproduced at the C and O *K* edges and some new peak assignments for these spectra were proposed. In order to examine the dynamical effect on the core-excited state and to understand the observed site-specific bond scission in PMMA and PiPac, the CHES MD simulations were performed. We found that the amount of the fragment ion is closely related to the character of the potential surface, i.e., the target bond length will be elongated or the yield of the fragment ion will be increased if the core-excited potential surface is repulsive. The features of the potential energy surface for the core-excited state depend strongly on the character of the chemical bond. Most of the potential energy surfaces corresponding to C–C single bonds are attractive, while at least one of the potential energy surfaces for the C–O bond is repulsive, leading to an accelerated C–O bond scission on this repulsive potential surface. Therefore, the existence of the repulsive potential is expected to contribute to the site-specific chemical reaction following core excitation.

From another point of view, it may be interesting to study the effect of the electronic charge transfer rate on both the core-hole and the Auger final states. Another important effect contributing to the chemical reaction following the core excitation is the bond breaking after the Auger decay, which has been discussed in a previous paper.⁷ In order to understand the generalities of the reactivity following the core excitation, not only the additional systematic theoretical calculations but also the experimental studies will be needed.

ACKNOWLEDGMENTS

The study was supported by a Grant-in-Aid on Research for the Future “Photoscience” from Japan Society for the Promotion of Science (JSPS-RFTF-98P01202) and the Grant-in-Aid from the Ministry of Education, Culture, Science, and Technology of Japan (15750011 and 16205002).

¹W. Eberhardt, T. K. Sham, R. Carr, S. Krummacher, M. Strongin, S. L. Weng, and D. Wesner, *Phys. Rev. Lett.* **40**, 1038 (1983).

²D. M. Hanson, *Adv. Chem. Phys.* **77**, 1 (1990).

³S. Nagaoka, K. Mase, and I. Koyano, *Trends Chem. Phys.* **6**, 1 (1997).

⁴T. Sekitani, E. Ikenaga, K. Fujii, K. Mase, N. Ueno, and K. Tanaka, *J. Electron Spectrosc. Relat. Phenom.* **101–103**, 135 (1999).

⁵T. Ibuki, K. Okada, K. Saito, and T. Gejo, *J. Electron Spectrosc. Relat. Phenom.* **107**, 39 (2000).

⁶E. Ikenaga, K. Kudara, K. Isari, S. A. Sardar, S. Wada, K. Mase, T. Sekitani, and K. Tanaka, *J. Electron Spectrosc. Relat. Phenom.* **114–116**, 585 (2001).

⁷E. O. Sako, Y. Kanameda, E. Ikenaga, M. Mitani, O. Takahashi, K. Saito, S. Iwata, S. Wada, T. Sekitani, and K. Tanaka, *J. Electron Spectrosc. Relat. Phenom.* **114–116**, 591 (2001).

⁸E. Ikenaga, K. Isari, K. Kudara, Y. Yasui, S. A. Sardar, S. Wada, T. Sekitani, K. Tanaka, K. Mase, and S. Tanaka, *J. Chem. Phys.* **114**, 2751 (2001).

⁹P. Bennich, T. Wiell, O. Karis, M. Weinelt, N. Wassdahl, A. Nilsson, M. Nyberg, L. G. M. Pettersson, J. Stöhr, and M. Samant, *Phys. Rev. B* **57**, 9274 (1998).

¹⁰K. Mase, M. Nagasono, S. Tanaka, T. Sekitani, and S. Nagaoka, *Fiz. Nizk. Temp.* **29**, 321 (2003).

¹¹S. Wada, E. O. Sako, R. Sumii, S. Waki, K. Isari, T. Sekiguchi, T. Sekitani, and K. Tanaka, *Nucl. Instrum. Methods Phys. Res. B* **199**, 361 (2003).

¹²S. Wada, R. Sumii, K. Isari, S. Waki, E. O. Sako, T. Sekiguchi, T. Sekitani, and K. Tanaka, *Surf. Sci.* **528**, 242 (2003).

¹³M. C. K. Tinone, K. Tanaka, J. Maruyama, N. Ueno, M. Imamura, and N.

Matsubayashi, *J. Chem. Phys.* **100**, 5988 (1994).

¹⁴D. Menzel and R. Gomer, *J. Chem. Phys.* **41**, 3311 (1964).

¹⁵P. A. Redhead, *Can. J. Phys.* **42**, 886 (1964).

¹⁶P. Antoniewicz, *Phys. Rev. B* **21**, 3811 (1980).

¹⁷D. E. Ramaker, C. T. White, and J. S. Murday, *J. Vac. Sci. Technol.* **18**, 748 (1981).

¹⁸D. E. Ramaker, C. T. White, and J. S. Murday, *Phys. Lett. A* **89**, 211 (1982).

¹⁹R. Guillemin, E. Shigemasa, K. Le Guen, D. Ceolin, C. Miron, N. Leclercq, P. Morin, and M. Simin, *Phys. Rev. Lett.* **87**, 203001 (2001).

²⁰K. Tanaka, E. O. Sako, E. Ikenaga, K. Isari, S. A. Sardar, S. Wada, T. Sekitani, K. Mase, and N. Ueno, *J. Electron Spectrosc. Relat. Phenom.* **119**, 255 (2001).

²¹T. E. Madey, D. E. Ramaker, and R. Stockbauer, *Annu. Rev. Phys. Chem.* **35**, 215 (1984).

²²V. Rehn and R. A. Rosenberg, in *Synchrotron Radiation Research: Advances in Surface and Interface Science*, edited by R. Z. Bachrach (Plenum, New York, 1984), Vol. 1, p. 327.

²³T. A. Carlson, *Photoelectron and Auger Spectroscopy* (Plenum, New York, 1975).

²⁴O. Takahashi, M. Mitani, M. Joyabu, K. Saito, and S. Iwata, *J. Electron Spectrosc. Relat. Phenom.* **120**, 137 (2001).

²⁵O. Takahashi, M. Joyabu, M. Mitani, K. Saito, and S. Iwata, *J. Comput. Chem.* **24**, 1329 (2003).

²⁶B. Brena, D. Nordlund, M. Odelius, H. Ogasawara, A. Nilsson, and L. G. M. Pettersson, *Phys. Rev. Lett.* **93**, 148302 (2004).

²⁷M. Odelius, H. Ogasawara, D. Nordlund *et al.*, *Phys. Rev. Lett.* **94**, 227401 (2005).

²⁸K. Fujii, H. Tomimoto, K. Isshiki, M. Tooyama, T. Sekitani, and K. Tanaka, *Jpn. J. Appl. Phys.* **38**, 321 (1999).

²⁹O. Takahashi, K. Saito, M. Mitani, H. Yoshida, F. Tahara, T. Sunami, K. Waki, Y. Senba, A. Hiraya, and L. G. M. Pettersson, *Jpn. J. Appl. Phys., Suppl.* **142**, 113 (2004).

³⁰R. Sankari, M. Ehara, H. Nakatsuji, Y. Senba, K. Hosokawa, H. Yoshida, A. De Faniis, Y. Tamenori, S. Aksela, and K. Ueda, *Chem. Phys. Lett.* **380**, 647 (2003).

³¹L. Triguero, L. G. M. Pettersson, and H. Ågren, *Phys. Rev. B* **58**, 8097 (1998).

³²C. Kolczewski, R. Püttner, O. Plashkevych *et al.*, *J. Chem. Phys.* **115**, 6426 (2001).

³³O. Takahashi and L. G. M. Pettersson, *J. Chem. Phys.* **121**, 10339 (2004).

³⁴M. Nyberg, M. Odelius, A. Nilsson, and L. G. M. Pettersson, *J. Chem. Phys.* **119**, 12577 (2003).

³⁵M. Cavalleri, H. Ogasawara, L. G. M. Pettersson, and A. Nilsson, *Chem. Phys. Lett.* **364**, 363 (2002).

³⁶Ph. Wernet, D. Nordlund, U. Bergmann *et al.*, *Science* **304**, 995 (2004).

³⁷M. J. Frisch, G. W. Trucks, H. B. Schlegel *et al.*, GAUSSIAN 98, Revision A.4 (Gaussian, Inc., Pittsburgh, PA, 1998).

³⁸L. G. M. Pettersson, H. Ågren, B. L. Schürmann, A. Lippitz, and W. E. S. Unger, *Int. J. Quantum Chem.* **63**, 749 (1997).

³⁹L. Triguero, O. Plashkevych, L. G. M. Pettersson, and H. Ågren, *J. Electron Spectrosc. Relat. Phenom.* **104**, 195 (1999).

⁴⁰J. C. Slater, *Adv. Quantum Chem.* **6**, 1 (1972).

⁴¹J. C. Slater and K. H. Johnson, *Phys. Rev. B* **5**, 844 (1972).

⁴²H. Ågren, V. Carravetta, O. Vahtras, and L. G. M. Pettersson, *Theor. Chem. Acc.* **97**, 14 (1997).

⁴³W. Hunt and W. A. Goddard III, *Chem. Phys. Lett.* **3**, 414 (1969).

⁴⁴H. Ågren, V. Carravetta, O. Vahtras, and L. G. M. Pettersson, *Chem. Phys. Lett.* **222**, 75 (1994).

⁴⁵L. G. M. Pettersson, U. Wahlgren, and O. Gropen, *Chem. Phys.* **80**, 7 (1983).

⁴⁶W. Kutzelnigg, U. Fleischer, and M. Schindler, *NMR-Basic Principles and Progress* (Springer-Verlag, Heidelberg, 1990).

⁴⁷K. Hermann, L. G. M. Pettersson, M. E. Casida, STOBE-DEMON, Version 2.0, STOBE software (2004).

⁴⁸J. P. Perdew and Y. Wang, *Phys. Rev. B* **33**, 8800 (1986).

⁴⁹P. E. Batson, *Phys. Rev. B* **48**, 2608 (1993).

⁵⁰K. C. Prince, L. Avaldi, M. Coreno, R. Camilloni, and M. de Simone, *J. Phys. B* **32**, 2551 (1999).

⁵¹S. Wada, H. Kizaki, Y. Matsumoto, R. Sumii, and K. Tanaka, *J. Phys.: Condens. Matter* (submitted).

⁵²T. X. Carroll, N. Berrah, J. Bozek, J. Hahne, E. Kukk, L. J. Sæthre, and T. D. Thomas, *Phys. Rev. A* **59**, 3386 (1999).